Int. J. Electrochem. Sci., 11**(2016)** 7333 – 7342, doi: 10.20964/2016.09.39

International Journal of ELECTROCHEMICAL SCIENCE
www.electrochemsci.org

Preparation and Electrochemical Performance of Modified $LiNi_{0.5}Mn_{1.5}O_4$Cathode Material for Lithium-ion Batteries

Xiaoling Tong, Min Zeng[*]*, Jing Li, Hui Xu,Meili Du, Fuyun Li*

School of Materials Science and Engineering, Southwest University of Science and Technology, Mianyang 621010, P R China
[*]E-mail: zengmin@swust.edu.cn

Received: 23 May2016/ *Accepted:* 7 July 2016 / *Published:* 7 August 2016

Modified $LiNi_{0.5}Mn_{1.5}O_4$-based materials with Cr-doped ($LiNi_{0.5}Mn_{1.4}Cr_{0.1}O_4$) and additional lithium ($Li_{1.1}Ni_{0.5}Mn_{1.4}Cr_{0.1}O_4$) have been synthesized by a solid-state method and their physicochemical and electrochemical performances have been investigated. The experimental results show that the Cr doping in $LiNi_{0.5}Mn_{1.4}Cr_{0.1}O_4$ and $Li_{1.1}Ni_{0.5}Mn_{1.4}Cr_{0.1}O_4$ suppresses the generation of Mn^{3+}, decreases the polarization, improves the conductivity and optimizes the cyclic performance and rate stability compared to the pristine $LiNi_{0.5}Mn_{1.5}O_4$. Besides, $Li_{1.1}Ni_{0.5}Mn_{1.4}Cr_{0.1}O_4$ delivers a higher discharge capacity of 108 mAh g^{-1} for the first cycle and 99 mAh g^{-1} after 50 cycles, which is much better than $LiNi_{0.5}Mn_{1.4}Cr_{0.1}O_4$ and $LiNi_{0.5}Mn_{1.5}O_4$. All these results show the vital role of the synergic effects between Cr^{3+} doping and additional lithium on the enhancement of electrochemical performance for $LiNi_{0.5}Mn_{1.5}O_4$, which will guide the development of $LiNi_{0.5}Mn_{1.5}O_4$-based cathode material in the future.

Keywords: Lithium-ion batteries; Cr-doped; additional lithium; $LiNi_{0.5}Mn_{1.5}O_4$ cathode;

1. INTRODUCTION

Future electric vehicles and other large electric power equipments require the development of large-scale high energy storage systems. Lithium-ion batteries (LIBs) are expected to be one of the most perspective candidates for this purpose due to their substantial features, such as high energy density, long lifespan, little self-discharge, memory-free effect and eco-friendly [1-4]. Cathode materials are an essential constituent in LIBs, however, the conventional $LiCoO_2$ cathode suffers from high cost and structural instability caused by degradation or failure when overcharged, which will prevent the future application of $LiCoO_2$ as a power battery cathode material [4-6]. To overcome these detrimental shortcomings and satisfy the increasing demands for large-scale energy storage, it is significant to develop novel high-performance cathode materials for LIBs. To date, spinel

$LiNi_{0.5}Mn_{1.5}O_4$ has received enormous interests due to its high output voltage (4.7V *vs* Li/Li^+), cost efficiency, environmental sustainable, low toxicity and rapid three-dimensional lithium-ion diffusion channels compared to the existing cathode materials [7-9].Unfortunately, the dissolution and Jahn-Teller distortion of Mn^{3+}, $LiNi_{0.5}Mn_{1.5}O_4$ could give rise to a rapid capacity decay and inferior cyclic performance [10, 11].

So far, numerous research have been developed to overcome these obstacles, ranging from cation doping [12-16] and synthesize additional lithium materials [1] to approaches including nanosizing [17-19] and coating [20-22]. In this manuscript, we utilize Cr^{3+} as a dopant not only due to its radius is approximate to Ni^{2+} and Mn^{4+}, but also the three electrons exist in its 3d energy level which retains less Jahn-Teller distortion [12]. In addition, Cr^{3+} diffuses into the $LiNi_{0.5}Mn_{1.5}O_4$ lattice and partially substitute for Mn^{4+} ions that could result in an increase of the hole concentration in $LiNi_{0.5}Mn_{1.5}O_4$, thus enhancing the electrical conductivity. In addition, a higher ratio of Li/Ni can produce an additional amount of lithium that could contribute to a larger capacity for $LiNi_{0.5}Mn_{1.5}O_4$. Electrochemical investigations disclose that our materials exhibit a high reversible capacity, excellent cyclic performance and great rate capability.

2. EXPERIMENTAL

2.1. Synthesis of lithium-rich and Cr-doped $Li_{1.1}Ni_{0.5}Mn_{1.4}Cr_{0.1}O_4$

$Li_{1.1}Ni_{0.5}Mn_{1.4}Cr_{0.1}O_4$ was synthesized by the traditional solid-state method. In brief, 1.03 g of Li_2CO_3, 0.94 g of NiO, 3.07 g of MnO_2 and 0.19 g Cr_2O_3 with a molar ratio of Li/Ni/Mn/Cr = 1.1/0.5/1.4/0.1 were milled homogeneously in an agate mortar. Then the homogeneous mixtures were annealed in air at 850 °C for 20h at a heating rate of 5 °C min^{-1}. Subsequently, the resultant products were milled again to adjust the particle size of the coarse particles caused by the high-temperature calcination. For comparison, $LiNi_{0.5}Mn_{1.4}Cr_{0.1}O_4$ and pristine $LiNi_{0.5}Mn_{1.5}O_4$ were also prepared in the same conditions, but with different Li/Ni/Mn/Cr ratio of 1/0.5/1.4/0.1 for $LiNi_{0.5}Mn_{1.4}Cr_{0.1}O_4$ and 1/0.5/1.5/0 for $LiNi_{0.5}Mn_{1.5}O_4$.

2.2. Materials Characterizations

The composition of each sample was calculate by Inductively coupled plasma (ICP) analysis on 6500 analyzer (ThermoFisher). Structural and crystallographic analyses of these samples were recorded by X-ray diffraction (XRD) with Cu-Kα radiation (X´Pert PRO, PANalytical) ranging from 10 to 80°. The particle size, morphology and elemental distribution of the products were examined by field emission scanning electron microscope (Ultra55, Zeiss) equipped with energy dispersive X-ray spectrometer (EDX).

2.3. Electrochemical Measurements

The working electrodes were prepared by milled the mixture of 80 wt % active materials with 10 wt % super P and 10 wt % polyvinylidene fluoride (PVDF) dissolved in N-methyl-2-pyrrolidone (NMP). Then this uniform slurry was coated onto aluminum foil and then dried at 120 °C for 24 h. Subsequently, these electrodes were cut into discs and assembled into CR2016 coin half cells in an Ar-filled glove box with Li foil as the negative electrodes and polypropylene microporous film (Celgard 2300) as the separators. The commercial electrolyte was brought from CAPCHEM in China. Galvanostatic charge and discharge measurement were operated on a LAND battery test system at 0.1C (1C=147 mAh g^{-1}) within the voltage of 3.5-5.0 V at room temperature. Electrochemical impedance spectroscopy (EIS) was performed on a CHI760C electrochemical station ranging from 0.01 Hz to 100 KHz.

3. RESULTS AND DISCUSSION

To identify the exact chemical compositions of Ni, Mn and Cr in the obtained samples, ICP measurement was conducted. Table 1 indicates that the chemical compositions of these samples are consistent with the stoichiometric ratio as designed. The XRD pattern of $LiNi_{0.5}Mn_{1.5}O_4$, $LiNi_{0.5}Mn_{1.4}Cr_{0.1}O_4$ and $Li_{1.1}Ni_{0.5}Mn_{1.4}Cr_{0.1}O_4$ is shown in Figure 1.

Table 1. Composition analysis data of the samples by the ICP data.

Material/element	Li	Ni	Mn	Cr
$LiNi_{0.5}Mn_{1.5}O_4$	0.98	0.5	1.49	—
$LiNi_{0.5}Mn_{1.4}Cr_{0.1}O_4$	0.98	0.5	1.39	0.098
$Li_{1.1}Ni_{0.5}Mn_{1.4}Cr_{0.1}O_4$	1.09	0.5	1.41	0.099

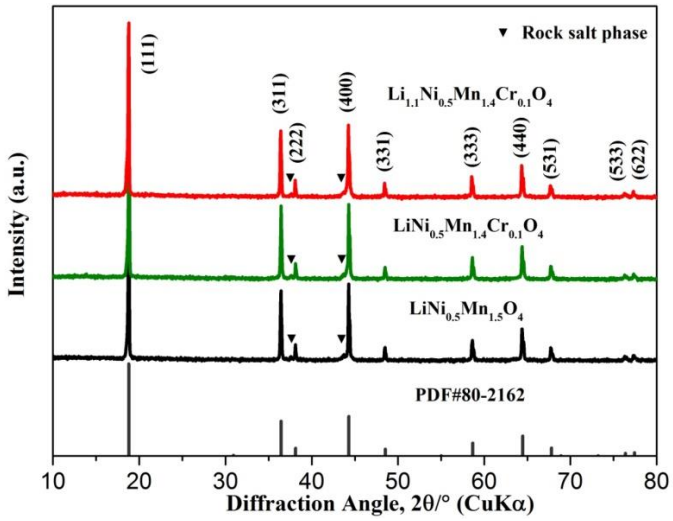

Figure 1. XRD patterns of$LiNi_{0.5}Mn_{1.5}O_4$, $LiNi_{0.5}Mn_{1.4}Cr_{0.1}O_4$ and $Li_{1.1}Ni_{0.5}Mn_{1.4}Cr_{0.1}O_4$.

The well-distinguished diffraction peaks of these samples assigned to the (111), (311), (400), and the other planes of the space group cubic $Fd\bar{3}m$ $LiNi_{0.5}Mn_{1.5}O_4$ (JCPDS No. 80-2162), consistent with previously reported data [23, 24]. This result implies that the doping and the additional lithium do not change the original $LiNi_{0.5}Mn_{1.5}O_4$ structure. However, very weak peaks at 2θ of 37.6° and 43.7° are detected in the XRD results for the samples of $LiNi_{0.5}Mn_{1.5}O_4$, $LiNi_{0.5}Mn_{1.4}Cr_{0.1}O_4$ and $Li_{1.1}Ni_{0.5}Mn_{1.4}Cr_{0.1}O_4$, which fit well with the rock-salt phase impurities ($Li_yNi_{1-y}O$) originated from the oxygen at high annealing temperatures above 750 ℃ [25, 26]. The lattice constants (cubic, a=b=c) of the samples were calculated according to the Scherrer formula and the results were 8.1880 Å, 8.1938 Å and 8.1986 Å for $LiNi_{0.5}Mn_{1.5}O_4$, $LiNi_{0.5}Mn_{1.4}Cr_{0.1}O_4$ and $Li_{1.1}Ni_{0.5}Mn_{1.4}Cr_{0.1}O_4$, respectively. This increases lattice parameter in $LiNi_{0.5}Mn_{1.4}Cr_{0.1}O_4$ results from the large radius of Cr^{3+} ~ 0.615 Å (*vs.* 0.53 Å of Mn^{4+}) and the additional lithium induced more Mn^{3+} (0.645 Å) reduced from Mn^{4+} in $Li_{1.1}Ni_{0.5}Mn_{1.4}Cr_{0.1}O_4$, due to charge compensation and leading to the increased lattice parameter, which consistent with the previous literatures [12, 26, 27]. Furthermore, the energy dispersive spectroscopy (EDS) images visually identify the uniform elemental distribution of Ni, Mn, Cr in $LiNi_{0.5}Mn_{1.4}Cr_{0.1}O_4$ and $Li_{1.1}Ni_{0.5}Mn_{1.4}Cr_{0.1}O_4$ (Figure 2).

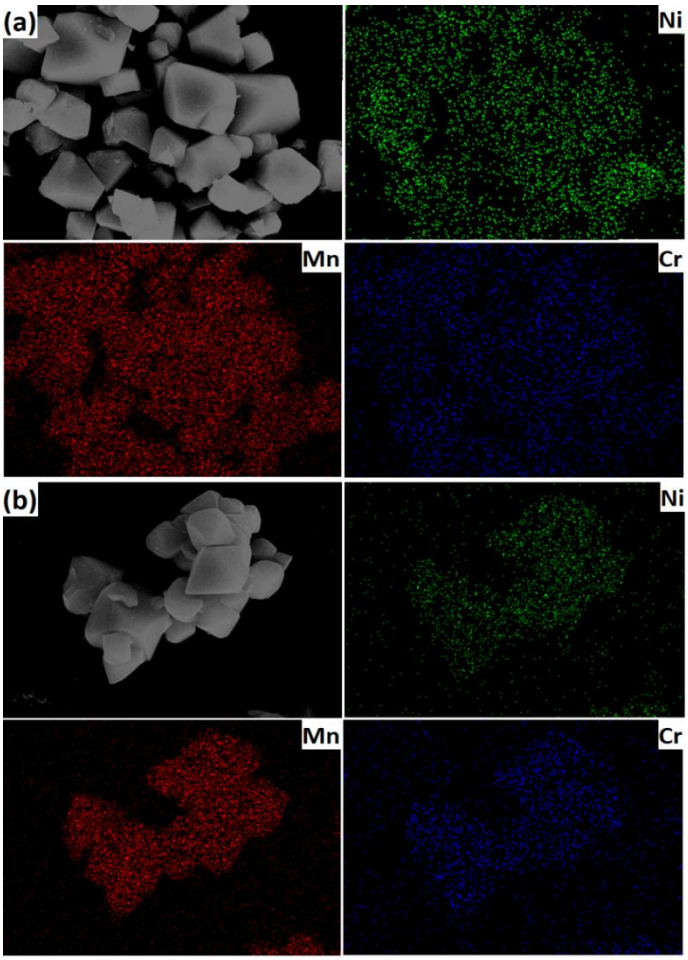

Figure 2. EDS mapping of Mn, Ni and Cr in (a) $LiNi_{0.5}Mn_{1.4}Cr_{0.1}O_4$, (b) $Li_{1.1}Ni_{0.5}Mn_{1.4}Cr_{0.1}O_4$.

Thus, it is reasonable to believe that the Cr^{3+} ions have been dispersed into the $LiNi_{0.5}Mn_{1.5}O_4$ lattice. Consequently, we believe this solid-state method to prepare the $LiNi_{0.5}Mn_{1.5}O_4$-based spinel materials is feasible.

The morphology and structure of $LiNi_{0.5}Mn_{1.5}O_4$, $LiNi_{0.5}Mn_{1.4}Cr_{0.1}O_4$ and $Li_{1.1}Ni_{0.5}Mn_{1.4}Cr_{0.1}O_4$ were illustrated by field emission scanning electron microscopy (FESEM), as shown in Figure 3. It can be seen that the Cr^{3+} doping plays an obvious impact on the surface morphology and particle size. The pristine $LiNi_{0.5}Mn_{1.5}O_4$ sample displays severe agglomeration, leading to a compact, large secondary particles, which are clearly composed of primary $LiNi_{0.5}Mn_{1.5}O_4$ particles, as shown in Figure 3 (a, d). These large agglomerated particles are detrimental to the diffusion for lithium ions and electrons because of the long diffusion pathway during the lithium-ion insertion/extraction process, which could result in inferior electrochemical performance of $LiNi_{0.5}Mn_{1.5}O_4$. In contrast, $LiNi_{0.5}Mn_{1.4}Cr_{0.1}O_4$ (Figure 3b, e) and $Li_{1.1}Ni_{0.5}Mn_{1.4}Cr_{0.1}O_4$ (Figure 3c, f) samples have small primary particles and most of them are octahedral-shaped. However, it is important to note that the $Li_{1.1}Ni_{0.5}Mn_{1.4}Cr_{0.1}O_4$ presents the smallest particle size in these samples and appears to distribute homogeneously. These results imply that the dopant of Cr^{3+} significantly reduce the particles agglomeration of the doped samples. Furthermore, the presence of additional lithium in the $Li_{1.1}Ni_{0.5}Mn_{1.4}Cr_{0.1}O_4$ can further reduce the agglomeration and improve homogeneity and the particle size is also decreased compared to $LiNi_{0.5}Mn_{1.4}Cr_{0.1}O_4$. The large surface area associated with the small particle size could facilitate the diffusion of electrolyte and significantly improve the kinetics of the lithium ions during intercalation/deintercalation process. We believe all these reasons will lead to an improved rate capability.

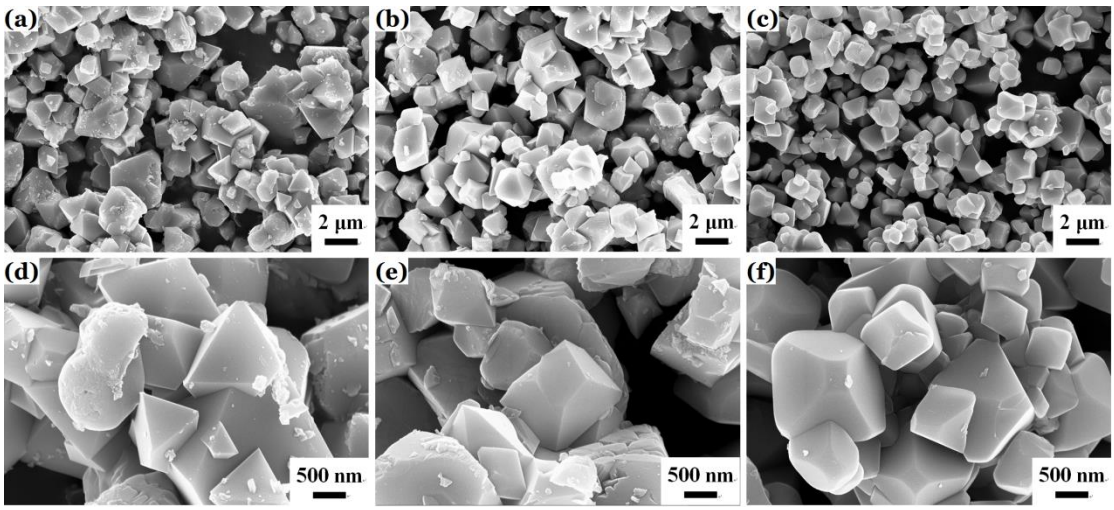

Figure 3. FESEM images of (a) (d) $LiNi_{0.5}Mn_{1.5}O_4$, (b) (e) $LiNi_{0.5}Mn_{1.4}Cr_{0.1}O_4$ and (c) (f) $Li_{1.1}Ni_{0.5}Mn_{1.4}Cr_{0.1}O_4$.

To evaluate the potential application of $Li_{1.1}Ni_{0.5}Mn_{1.4}Cr_{0.1}O_4$ and $LiNi_{0.5}Mn_{1.4}Cr_{0.1}O_4$ as LIBs cathodes, galvanostatic tests were performed at 0.1 C (1 C = 147 mAh g^{-1}) between the voltage window of 3.5-5.0 V (*vs*. Li/Li^+), as seen in Figure 4.

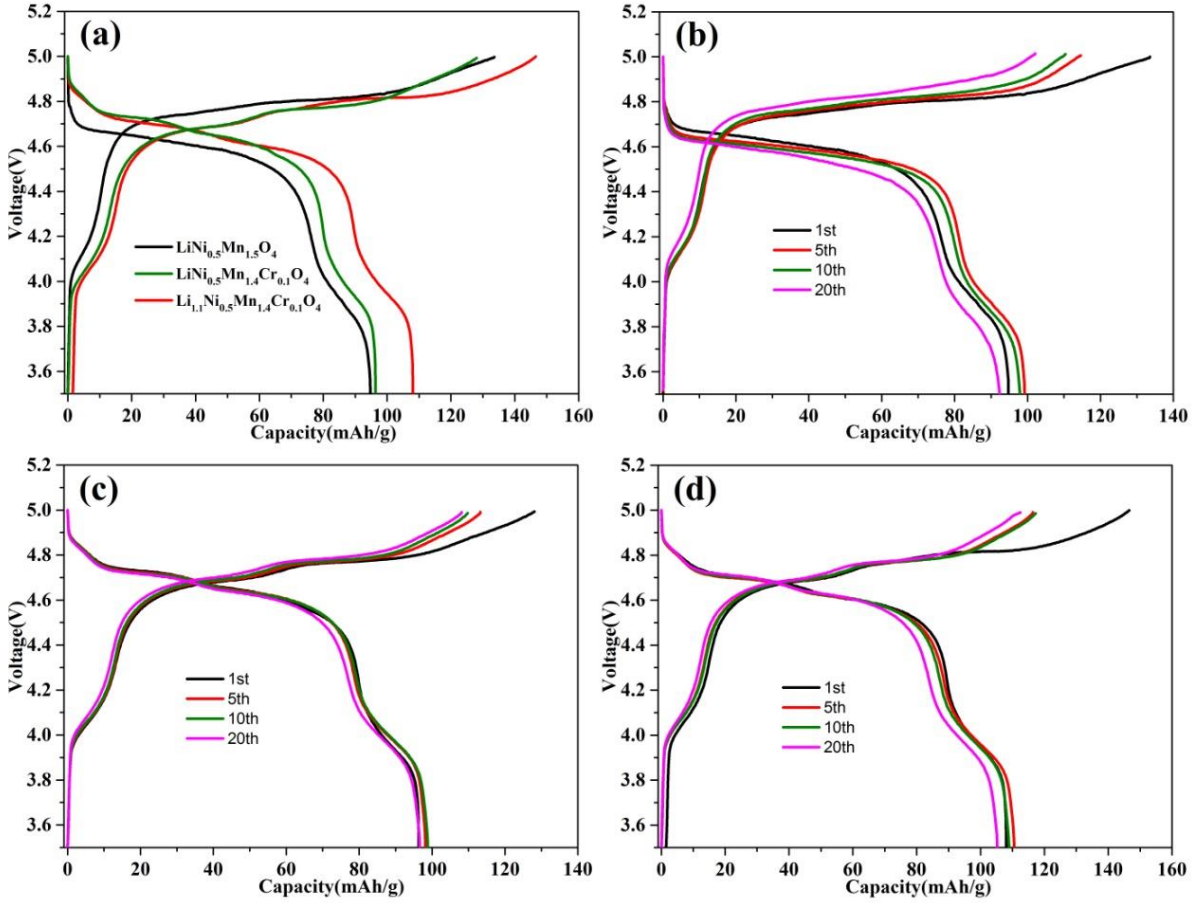

Figure 4. (a) The first charge/discharge curves of three samples. The 1st, 5th, 10th, 20th charge/discharge curves of (b) $LiNi_{0.5}Mn_{1.5}O_4$, (c) $LiNi_{0.5}Mn_{1.4}Cr_{0.1}O_4$ and (d) $Li_{1.1}Ni_{0.5}Mn_{1.4}Cr_{0.1}O_4$.

Table 2. Comparison of charge capacities and Mn^{3+} contents in the samples.

Sample	Capacity in 4V region (mAh g^{-1})	Amount of Mn^{3+}(%)
$LiNi_{0.5}Mn_{1.5}O_4$	17.50	18.47%
$LiNi_{0.5}Mn_{1.4}Cr_{0.1}O_4$	16.42	17.04%
$Li_{1.1}Ni_{0.5}Mn_{1.4}Cr_{0.1}O_4$	18.66	17.27%

The first charge and discharge curves is shown in Figure 4a, a long voltage plateaus at 4.6−4.8 V stems from Ni^{2+}/Ni^{3+}, Ni^{3+}/Ni^{4+} and a minor sloping plateau around 4.1 V can be ascribe to the Mn^{3+}/Mn^{4+} redox couple, respectively [28, 29]. This phenomenon further confirms the crystal structures of our samples are disordered $Fd\bar{3}m$, consistent with the result of XRD [29]. In addition, the two plateaus at 4.6 and 4.8 V become more obvious and the gap is larger in the Cr^{3+} doping samples , which testifies that the Cr^{3+} doping increases the cationic disorder [26]. Moreover, all the samples show the low columbic efficiency which could ascribe to the decomposition of the electrolyte at high operation voltage [30]. To confirm the content of Mn^{3+}, detailed calculation was conducted according to the capacity percentage contribution from the 4 V plateau of the initial discharge capacity (Figure.

4a) for the samples, as shown in Table 2. The capacities contributed by Mn^{3+} for $LiNi_{0.5}Mn_{1.5}O_4$, $LiNi_{0.5}Mn_{1.4}Cr_{0.1}O_4$ and $Li_{1.1}Ni_{0.5}Mn_{1.4}Cr_{0.1}O_4$ are 18.47, 17.04, 17.27%, respectively, indicating that Cr^{3+} suppress the formation of Mn^{3+}. However, the Mn^{3+} content in $Li_{1.1}Ni_{0.5}Mn_{1.4}Cr_{0.1}O_4$ is higher than that of $LiNi_{0.5}Mn_{1.4}Cr_{0.1}O_4$, which may be due to the charge compensation of the additional lithium ions existed in +1 oxidation state lowers the average manganese valence, leading to the more Mn^{3+} reduced from Mn^{4+}, consistent with the result of XRD. This observation is good agreement with the previous reporters [1, 26].

To further study the effect of Cr^{3+}, we compared the curves of 1st, 5th, 10th and 20th of the samples, as shown in Figure 4b−d. Results indicate that the Cr^{3+} decreases the polarization of $LiNi_{0.5}Mn_{1.4}Cr_{0.1}O_4$ and $Li_{1.1}Ni_{0.5}Mn_{1.4}Cr_{0.1}O_4$ than that of $LiNi_{0.5}Mn_{1.5}O_4$ [30]. The initial discharge capacities are 95, 96, and 108 mAh g^{-1} for $LiNi_{0.5}Mn_{1.5}O_4$, $LiNi_{0.5}Mn_{1.4}Cr_{0.1}O_4$ and $Li_{1.1}Ni_{0.5}Mn_{1.4}Cr_{0.1}O_4$, respectively. We conclude that Cr^{3+} make little contribution to the capacity, whereas the addtional lithium in $Li_{1.1}Ni_{0.5}Mn_{1.4}Cr_{0.1}O_4$ increases the capacity about 12.0 %, which is higher than that of $LiNi_{0.5}Mn_{1.4}Cr_{0.1}O_4$, consistent with the result of Table 1.

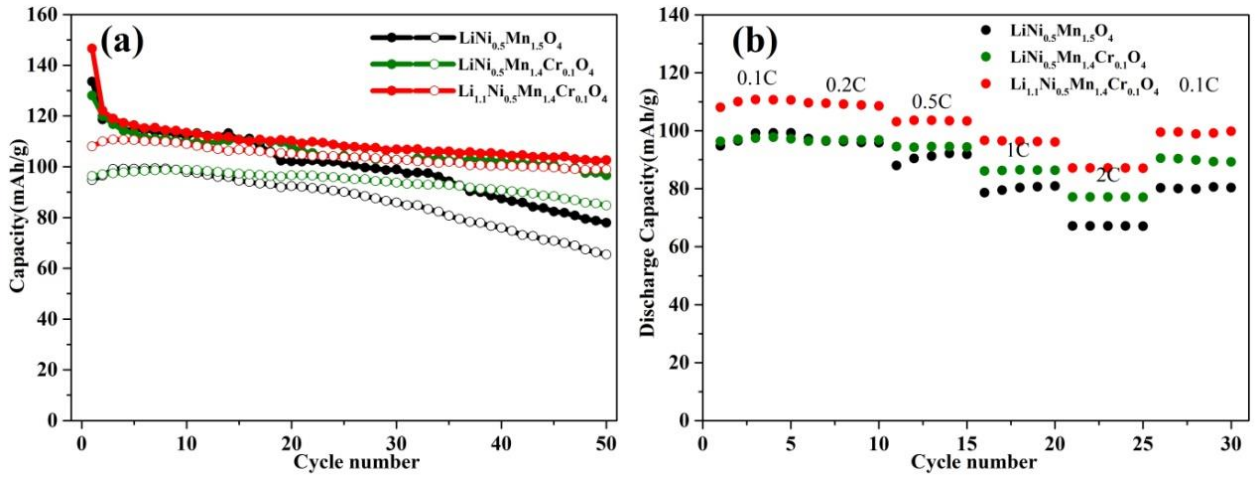

Figure 5. (a) Cyclic performance, (b) rate capability of $LiNi_{0.5}Mn_{1.5}O_4$, $LiNi_{0.5}Mn_{1.4}Cr_{0.1}O_4$ and $Li_{1.1}Ni_{0.5}Mn_{1.4}Cr_{0.1}O_4$.

Figure 5a displays the cyclic performance of the three samples at 0.1 C and the discharge capacities of 65, 85, and 99 mAh g^{-1} are obtained after 50 cycles at room temperature for $LiNi_{0.5}Mn_{1.5}O_4$, $LiNi_{0.5}Mn_{1.4}Cr_{0.1}O_4$ and $Li_{1.1}Ni_{0.5}Mn_{1.4}Cr_{0.1}O_4$, with the corresponding capacity retention ratios of 69, 88 and 92 %, respectively. The discharge capacity is dramatically decreased after 34 cycles in $LiNi_{0.5}Mn_{1.5}O_4$, whereas $LiNi_{0.5}Mn_{1.4}Cr_{0.1}O_4$ and $Li_{1.1}Ni_{0.5}Mn_{1.4}Cr_{0.1}O_4$ display better cyclic performance. These results imply that Cr^{3+} enhances the cyclic stability of modified $LiNi_{0.5}Mn_{1.5}O_4$. The reversible capacity of $Li_{1.1}Ni_{0.5}Mn_{1.4}Cr_{0.1}O_4$ is higher than that of the others, which may be attributed to the synergistic effect of the additional lithium, high Mn^{3+} content and the large cationic disorder [26, 27].

The rate capability of the as-prepared samples was performed at different rates from 0.1 C to 2 C for every 5 successive cycles, as shown in Figure 5b. $Li_{1.1}Ni_{0.5}Mn_{1.4}Cr_{0.1}O_4$ delivered a discharge capacity of 111 mAh g^{-1} for the 5^{th} cycle at 0.1 C, whereas $LiNi_{0.5}Mn_{1.4}Cr_{0.1}O_4$ and $LiNi_{0.5}Mn_{1.5}O_4$ only kept at 98 and 99 mAh g^{-1}, respectively. The following discharge capacities of the $Li_{1.1}Ni_{0.5}Mn_{1.4}Cr_{0.1}O_4$, $LiNi_{0.5}Mn_{1.4}Cr_{0.1}O_4$ and $LiNi_{0.5}Mn_{1.5}O_4$ electrodes at different rates were 109, 97 and 96 mAh g^{-1} for the 10^{th} cycle at 0.2 C, 103, 94, and 92 mAh g^{-1} for the 15^{th} cycle at 0.5 C, 96, 86, and 81 mAh g^{-1} for the 20^{th} cycle at 1 C, and 87, 77, and 67 mAh g^{-1} for the 25^{th} cycle at 2 C, respectively. Moreover, when the rate restored to the initial current density of 0.1 C after 30 cycles, $Li_{1.1}Ni_{0.5}Mn_{1.4}Cr_{0.1}O_4$ and $LiNi_{0.5}Mn_{1.4}Cr_{0.1}O_4$ kept at 100 and 89 mAh g^{-1}, whereas $LiNi_{0.5}Mn_{1.5}O_4$ only maintained at 80 mAh g^{-1}, with 92.6, 92.7 and 84.2% of the initial reversible capacity. These results reveal that Cr^{3+} plays a significant role on enhancing the rate capability of $LiNi_{0.5}Mn_{1.5}O_4$. These phenomena may be due to the Cr^{3+} that increases the charge vacancy induced by the electric neutrality in the lattice and the larger cationic disorder could increase the lithium ion diffusion coefficient and enhance the electronic conductivity of $LiNi_{0.5}Mn_{1.4}Cr_{0.1}O_4$ and $Li_{1.1}Ni_{0.5}Mn_{1.4}Cr_{0.1}O_4$ [26]. Moreover, the large amount of Mn^{3+} resulted from the additional lithium in $Li_{1.1}Ni_{0.5}Mn_{1.4}Cr_{0.1}O_4$ may increase its conductivity, and the small homogeneous particles with high specific surface area that could facilitate the migration of lithium ions and electron. These features make the $Li_{1.1}Ni_{0.5}Mn_{1.4}Cr_{0.1}O_4$ process superior rate capability than the others. In order to investigate the electrical conductivity of these samples, electrochemical impedance spectroscopy (EIS) measurements were carried out, as shown in Figure 6.

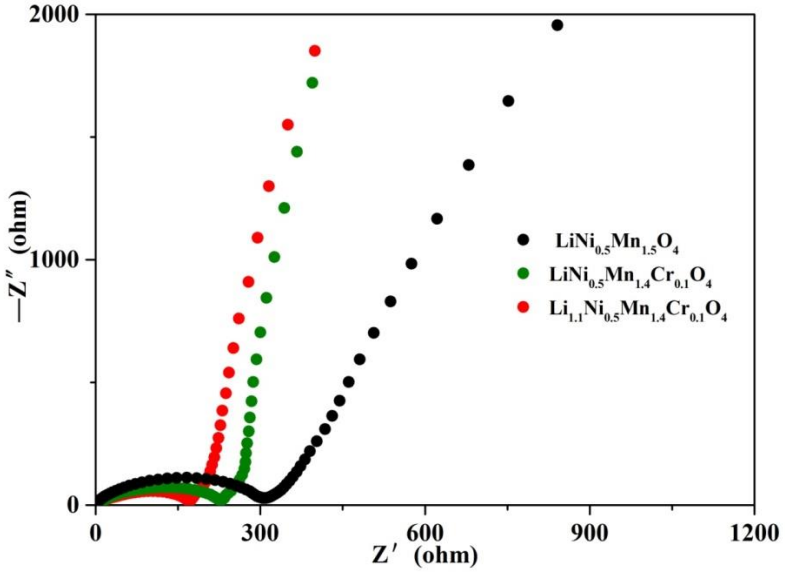

Figure 6. Electrochemical impedance spectra of $LiNi_{0.5}Mn_{1.5}O_4$, $LiNi_{0.5}Mn_{1.4}Cr_{0.1}O_4$ and $Li_{1.1}Ni_{0.5}Mn_{1.4}Cr_{0.1}O_4$.

The similar intercept of these samples on the abscissa axis reveals the similar impedance of electron conductivity and Li^+ conductivity in the electrolyte. The semicircle diameter of

$Li_{1.1}Ni_{0.5}Mn_{1.4}Cr_{0.1}O_4$ is the smallest than the others reflects that the smallest charge-transfer impedance across the solid/electrolyte interface due to the high specific surface area which is in favor of the transportation of lithium-ion and electron. Lithium-ion diffusion impedance of $Li_{1.1}Ni_{0.5}Mn_{1.4}Cr_{0.1}O_4$ and $LiNi_{0.5}Mn_{1.4}Cr_{0.1}O_4$ is lower than $LiNi_{0.5}Mn_{1.5}O_4$ in the solid, corresponding to the gradient of oblique line at low frequencies. This result fits well with the lattice constant (8.188 Å-$LiNi_{0.5}Mn_{1.5}O_4$, 8.1938 Å -$LiNi_{0.5}Mn_{1.4}Cr_{0.1}O_4$ and 8.1986 Å -$Li_{1.1}Ni_{0.5}Mn_{1.4}Cr_{0.1}O_4$), that is, the larger lattice constant, the faster the lithium-ion transport [23]. Hence, the $Li_{1.1}Ni_{0.5}Mn_{1.4}Cr_{0.1}O_4$ electrodes show excellent rate capability compared to the $LiNi_{0.5}Mn_{1.4}Cr_{0.1}O_4$ and $LiNi_{0.5}Mn_{1.5}O_4$.

4. CONCLUSIONS

In summary, we synthesize modified $LiNi_{0.5}Mn_{1.5}O_4$ of $LiNi_{0.5}Mn_{1.4}Cr_{0.1}O_4$ and $Li_{1.1}Ni_{0.5}Mn_{1.4}Cr_{0.1}O_4$ by a solid state method as high performance cathode materials for LIBs. The as-prepared $LiNi_{0.5}Mn_{1.4}Cr_{0.1}O_4$ and $Li_{1.1}Ni_{0.5}Mn_{1.4}Cr_{0.1}O_4$ electrodes exhibit excellent cyclic and rate performance, which are much better than that of the $LiNi_{0.5}Mn_{1.5}O_4$ electrodes. The excellent electrochemical performance can be ascribed to the Cr^{3+} that could enhance the electronic conductivity and the larger cationic disorder could increase the lithium ion diffusion coefficient of $LiNi_{0.5}Mn_{1.4}Cr_{0.1}O_4$ and $Li_{1.1}Ni_{0.5}Mn_{1.4}Cr_{0.1}O_4$. In addition, the additional lithium, high Mn^{3+} content and the small homogeneous particles further enhance the rate capability of the $Li_{1.1}Ni_{0.5}Mn_{1.4}Cr_{0.1}O_4$. Therefore, it is reasonable to conclude that the $Li_{1.1}Ni_{0.5}Mn_{1.4}Cr_{0.1}O_4$ with Cr^{3+} doping and extra amount of lithium is very promising for application as cathodes in LIBs.

References

1. J. Hassoun, K. S. Lee, Y. K. Sun and B. Scrosati, *J. Am. Chem. Soc.*, 133 (2011) 3139.
2. F. Y. Li, M. Zeng, J. Li, X. L. Tong, H. Xu, *RSC Adv.*, 6 (2016) 26902.
3. K. X. Wang, X. H. Li and J. S. Chen, *Adv. Mater.*, 27 (2015) 527.
4. H. Xu, M. Zeng, J. Li and X. L. Tong, *RSC Adv.*, 5 (2015) 91493.
5. H. W. Choi, S. J. Kim, Y. H. Rim and Y. S. Yang, *J. Phys. Chem. C*, 119 (2015) 27192.
6. X. W. Gao, Y. F. Deng, D. Wexler, G. H. Chen, S. L. Chou, H. K. Liu, Z. C. Shi and J. Z. Wang, *J. Mater. Chem. A*, 3 (2015) 404.
7. N. Nitta, F. X. Wu, J. T. Lee and G. Yushin, *Mater. Today*, 18 (2015) 252.
8. H. M. Cho, M. V. Chen, A. C. MacRae and Y. S. Meng, *ACS Appl. Mater. Inter.*, 7 (2015) 16231.
9. X. L. Zhang, F. Y. Cheng, J. G. Yang and J. Chen, *Nano Lett.*, 13 (2013) 2822.
10. D. Liu, W. Zhu, J. Trottier, C. Gagnon, F. Barray, A. Guerfi, A. Mauger, H. Groult, C. M. Julien, J. B. Goodenough and K. Zaghib, *RSC Adv.*, 4 (2014) 154.
11. C. Liu, Z. Y. Wang, C. S. Shi, E. Z. Liu, C. N. He and N. Q. Zhao, *ACS Appl. Mater. Inter.*, 6 (2014) 8363.
12. S. H. Oh, S. H. Jeon, W. Cho, C. S. Kim and B. W. Cho, *J. Alloy. Compd.*, 452 (2008) 389.
13. H. L. Wang, T. A. Tan, P. Yang, M. O. Lai and L. Lu, *J. Phys. Chem. C*, 115 (2011) 6102.
14. M. H. Liu, H. T. Huang, C. M. Lin, J. M. Chen and S. C. Liao, *Electrochim. Acta*, 120 (2014) 133.
15. J. Liu and A. Manthiram, *J. Phys. Chem. C*, 113 (2009) 15073.
16. G. B. Zhong, Y. Y. Wang, X. J. Zhao, Q. S. Wang, Y. Yu and C. H. Chen, *J. Power Sources*, 216 (2012) 368.
17. S. K. Hong, S. Mho, I. H. Yeo, Y. K. Kang and D. W. Kim, *Electrochim. Acta*, 156 (2015) 29.

18. Z. X. Chen, S. Qiu, Y. L. Cao, X. P. Ai, K. Xie, X. B. Hong and H. X. Yang, *J. Mater. Chem.*, 22 (2012) 17768.
19. X. L. Zang, F. Y. Cheng, K. Zhang, Y. L. Liang, S. Q. Yang, J. Liang and J. Chen, *RSC Adv.*, 2 (2012) 5669.
20. J. W. Kim, D. H. Kim, D. Y. Oh, H. Lee, J. H. Kim, J. H. Lee and Y. S. Jung, *J. Power Sources*, 274 (2015) 1254.
21. H. M. Wu, I. Belharouak, A. Abouimrane, Y. K. Sun and K. Amine, *J. Power Sources*, 195 (2010) 2909.
22. D. L. Liu, Y. Bai, S. Zhao and W. F. Zhang, *J. Power Sources*, 219 (2012) 333.
23. M. Kunduraci and G. G. Amatucci, *J. Electrochem. Soc.*, 153 (2006) 1345.
24. Y. Talyosef, B. Markovsky, R. Lavi, G. Salitra, D. A. D. Kovacheva, M. Gorova, E. Zhecheva and R. Stoyanova, *J. Electrochem. Soc.*, 154 (2007) 682.
25. H. F. Luo, P. Nie, L. F. Shen, H. S. Li, H. F. Deng, Y. Y. Zhu and X. G. Zhang, *ChemElectroChem*, 2 (2015) 127.
26. L. N. Wan, Y. F. Deng, C. X. Yang, H. Xu, X. S. Qin and G. H. Chen, *RSC Adv.*,5 (2015) 25988.
27. J. Xiao, X. L. Chen, P. V. Sushko, M. L. Sushko, L. Kovarik, J. J. Feng, Z. Q. Deng, J. M. Zheng, G. L. Graff, Z. M. Nie, D. W. Choi, J. Liu, J. G. Zhang and M. S. Whittingham, *Adv. Mater.*, 24 (2012) 2109.
28. X. Fang, M. Y. Ge, J. P. Rong and C. W. Zhou, *ACS Nano*, 8 (2014) 4876.
29. J. C. Li, Q. L. Zhang, X. C. Xiao, Y. T. Cheng, C. D. Liang and N. J. Dudney, *J. Am. Chem. Soc.*, 137 (2015) 13732.
30. D. Liu, C. Gagnon, J. Trottier, A. Guerfi, D. Clement, P. Hovington, A. Mauger, C. M. Julien and K. Zaghib, *Electrochem. Commun*., 41 (2014) 64.